

Assessment of constant-potential implicit solvation calculations of electrochemical energy barriers

Maxime Van den Bossche,^{†,‡} Egill Skúlason,[‡] Christoph Rose-Petruck,[†] and Hannes Jónsson^{*,‡}

[†]*Department of Chemistry, Brown University, Providence, RI, United States*

[‡]*Science Institute and Faculty of Physical Sciences, University of Iceland, 107 Reykjavík, Iceland*

E-mail: hj@hi.is

Abstract

Theoretical estimation of the activation energy of electrochemical reactions is of critical importance but remains challenging. In this work, we address the usage of an implicit solvation model for describing hydrogen evolution reaction steps on Pt(111) and Pt(110), and compare with the ‘extrapolation’ approach and co-workers as well as single-crystal measurements. We find that both methods yield qualitatively similar results, which are in fair agreement with the experimental data. Care should be taken, however, in addressing spurious electrostatic interactions between periodically repeated slabs in the VASPsol implementation. Considering the lower computational cost and higher flexibility of the implicit solvation approach, we expect this method to become a valuable tool in electrocatalysis.

Introduction

Electrocatalytic reactions involve electron transfer to or from an electrode surface and are evidently crucial for all electrochemical production processes, as well as for corrosion chemistry and the electronics industry. Detailed insights into the reaction mechanism and kinetics, however, are difficult to obtain and

generally require a combination of experimental and computational work.

While in classical, “gas phase” heterogeneous catalysis the field of theoretical modeling is rather well established, further methodological development is still required when it comes to electrocatalysis. Two major challenges in this field are given by (i) the description of metal/electrolyte interface, and (ii) the requirement of constant electrode potential over the course of an electron transfer reaction. These aspects complicate, in particular, the evaluation of activation energies of electron transfer reactions. As a result, the vast majority of computational electrocatalysis studies have been limited to thermodynamic properties only, such as reaction energies.^{1,2} It is, however, well recognized that the proper study of reaction kinetics (in electrocatalysis as in conventional catalysis) requires knowledge of transition state energies.^{3,4}

Several approaches have so far been proposed to address these challenges, which differ especially in the manner the constant-potential requirement is handled. This requirement stipulates that the electrode potential w.r.t. the reference electrode remains constant over the course of an elementary reaction, also when it is accompanied by electron transfer. As only a finite number of electrons N_e can be included in

the electronic structure calculations, however, the potential will change significantly over the course of an electron transfer reaction, if N_e is held constant.⁵⁻⁷ Extended electrode surfaces are furthermore most conveniently modeled using periodically repeated supercells, which must satisfy overall charge neutrality.

In this context, the arguably most rigorous method is the so-called ‘extrapolation’ approach,^{5,6} where energy barriers are evaluated at successively larger lateral cell dimensions and extrapolated to the infinite cell limit where the potential drop is zero. The number of electrons N_e is determined by the charge neutrality condition, which entails that e.g. hydrogen atoms must be added to or withdrawn from the electrolyte to vary the electrode potential. This method has so far exclusively been applied to FCC(111) surfaces in conjunction with ice-like hexagonal water structures.^{5,6,8,9}

In a second, related method,^{10,11} the computationally costly extrapolation is avoided by assuming that the required correction to the transition state energy has a purely capacitive character. This correction is based on changes in the charges of the metal atoms at the electrode surface, and hence an additional ambiguity lies in the choice of the charge density partitioning scheme.

Thirdly, in the ‘double reference’ approach^{12,13} the electrode potential is controlled by varying N_e , with introduction of a homogeneous compensating background to maintain overall charge neutrality. It is not quite clear, at this point, if this method applies sound corrections to the obtained total energies, which is known to be a non-trivial problem in the case of charged slabs in homogeneous compensating backgrounds.^{14,15}

Methods have also been proposed where charge neutrality is maintained by localizing the compensating charge in a ‘counter-electrode’ at some distance away from the electrode/electrolyte interface.^{16,17} In reality, however, charge compensation is mediated by changes in the concentration profiles of the electrolyte’s ions near the electrode surface.

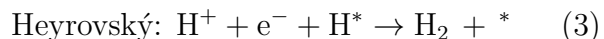
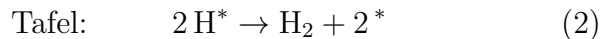
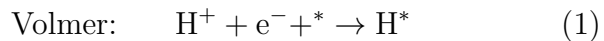
In yet another approach^{18,19} electrochemical barriers are estimated in a two-step pro-

cedure inspired by Marcus theory. First, the activation energy of the corresponding non-electrochemical reaction is calculated (e.g. reaction with adsorbed H in the case of a proton-coupled electron transfer (PCET) reaction) and it is assumed that, at the same potential, the electrochemical process possesses the same activation energy. The potential dependence of the activation energy is then described using e.g. Butler-Volmer theory, requiring further simplifying assumptions regarding the symmetry factor of the reaction.

Finally, a more recently developed approach, which we will be focusing on in this work, is one where (part of) the electrolyte is approximated by a polarizable dielectric continuum (i.e. an implicit solvation model).²⁰⁻²³ The constant-potential requirement is here obeyed by varying N_e with concomitant changes in the concentration of counterions in the surrounding electrolytes (frequently described by Poisson-Boltzmann theory). The main assumption here, then, is that the ionic distribution in the electrolyte is equilibrated also at the saddle point, and not only at the reactant and product states.

Although several studies have applied the above constant-potential approach with implicit solvation models (using e.g. the VASP-sol,²⁴⁻²⁷ JDFTx,²⁸ SIESTA²⁹⁻³³ and GPAW codes³⁴), we are not aware of attempts to compare its results to those of the extrapolation method, or to detailed single-crystal measurements.

The present work offers such a comparison, focusing on the various steps of the hydrogen evolution reaction (HER) on Pt(111) and Pt(110). There are three types of reactions relevant to the HER:



Adsorbed H and vacant adsorption sites are denoted H^* and $*$, respectively.

The (111) facet is chosen to compare with the extrapolation approach, which has so far been exclusively applied to FCC(111) surfaces due to

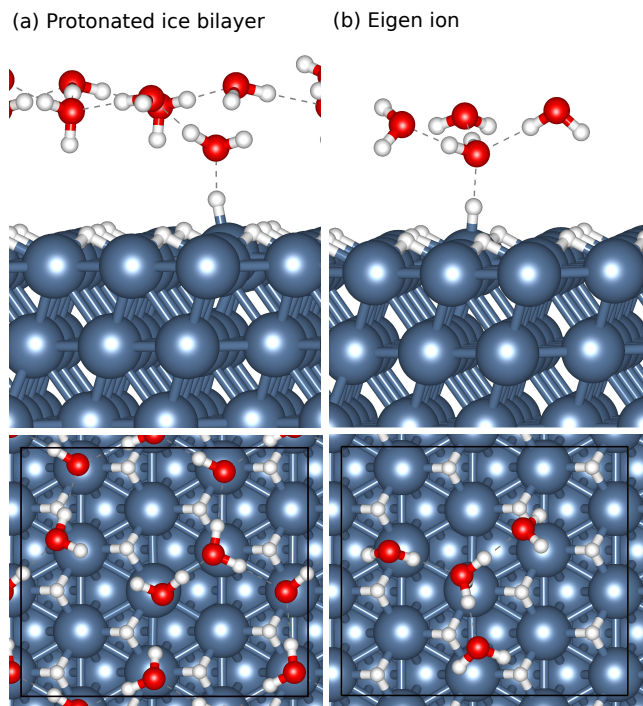


Figure 1: Side and top views of the obtained transition states for the Volmer reaction on Pt(111) at an initial hydrogen coverage of 0.92 ML. The considered water structure are a protonated hexagonal ice bilayer [Panel (a)] and a $\text{H}_3\text{O}^+(\text{H}_2\text{O})_3$ (‘Eigen’) cation [Panel (b)].

the commensurability with the hexagonal ice bilayer structure used to model the metal/water interface. The structure of this adlayer is illustrated in Figure 1, in the transition state for hydrogen deposition via the Volmer reaction. As the implicit solvation approach is less restricted in terms of water structures, we will also compare with results from a water cluster model, corresponding to the ‘Eigen’ cation in its protonated form ($\text{H}_3\text{O}^+(\text{H}_2\text{O})_3$). Also the HER steps on (110) facets are included, as experimental Tafel slopes are here easier to analyze and indicate a Volmer-Tafel mechanism with the Tafel reaction as the rate-determining step (RDS).³⁵

It should be noted that the above considerations apply not only to activation energies but also to reaction energies. The latter have, however, typically been calculated using the computational hydrogen electrode (CHE) formalism,¹ which makes use of the equilibrium relation of the proton/hydrogen redox-couple of the standard hydrogen electrode (SHE). The focus of

this work will hence lie on the estimation of barrier heights.

Computational methods

To facilitate the comparison to results from previous publications with the extrapolation approach,⁶ the same computational setup is used here. The bulk of the electronic structure calculations are performed with the VASP code^{36–39} using Kohn-Sham density functional theory (DFT).^{40,41} Core electrons are treated via standard projector augmented wave (PAW) setups with the following valences: H (1), O (6), Pt (10). The basis set consists of plane waves with a kinetic energy up to 350 eV.

Additional calculations are carried out using the JDFTx code²¹ using GBRV ultrasoft pseudopotentials⁴² with the recommended cutoffs for the wave functions (20 Hartree) and the electron density (100 Hartree).¹

Electronic exchange and correlation are described using the revised Perdew-Burke-Ernzerhof (RPBE) functional⁴³ which modifies the exchange enhancement factor of the original PBE expression⁴⁴ to improve the description of adsorption energies on transition metal surfaces. In JDFTx the RPBE functional is implemented through the LibXC library.⁴⁵

Three-layer slabs of $c(3 \times 4)$ geometry are employed for the Pt(111) surface, with the RPBE crystal lattice constant of 4.025 Å. For the Pt(110) slab, six metal layers are used with a $p(2 \times 4)$ cell size and a (1×2) missing-row reconstruction. In both cases the first Brillouin zone is sampled using $(4 \times 3 \times 1)$ Monkhorst-Pack grids.^{46,47} Local minimizations and saddle point searches with the dimer method^{48,49} are pursued until the largest force components are less than 0.05 eV/Å in magnitude. All metal layers except the topmost layer are constrained to their bulk lattice positions. The distances separating periodically repeated slabs will be addressed in the Results section.

Implicit solvation calculations of the aqueous electrolyte are performed using the GLSSA13

¹In the GBRV pseudopotential set the $5p^6$ semicore states are included in the valence for Pt.

solvent model,⁵⁰ which is available in VASP through the VASPsol extension.^{22,23} Like other models such as SCCS,⁵¹ the method puts forward a dielectric profile ϵ as a functional of the Kohn-Sham electron density distribution ρ :

$$\epsilon[\rho] = 1 + (\epsilon_{\text{bulk}} - 1) S[\rho], \quad (4)$$

with the following form for the ‘shape function’ S :

$$S[\rho] = \frac{1}{2} \text{erfc} \left(\frac{\log(\rho/\rho_{\text{cut}})}{\sigma\sqrt{2}} \right). \quad (5)$$

The dielectric function therefore changes gradually from 1 to the bulk dielectric constant ϵ_{bulk} (78.4, the experimental value for liquid water at 298 K⁵²). The particular shape of this transition is governed by the σ and ρ_{cut} parameter, for which we have applied the default values (0.6 and 0.0025 Å⁻³, respectively). The free energy required to create a solvent cavity around the solute is calculated as

$$A_{\text{cavity}} = \tau \int |\nabla S| d\mathbf{r}, \quad (6)$$

where the τ parameter (0.525 meV/Å²) has been optimized to reproduce the solvation energies of a series of organic molecules.²²

In case the electrode potential is different from the potential of zero charge (PZC), a counterion charge distribution is included in the implicit solvent region through the use of the generalized Poisson-Boltzmann equation:

$$\nabla \cdot \epsilon(\mathbf{r}) \nabla \phi_{\text{tot}}(\mathbf{r}) = \left(\frac{2c_0 q^2 e^2}{k_B T} \right) \phi_{\text{tot}}(\mathbf{r}) - \rho_{\text{solute}}(\mathbf{r}), \quad (7)$$

$$c_{\pm}(\mathbf{r}) = c_0 \exp \left(\frac{\pm q e \phi_{\text{tot}}(\mathbf{r})}{k_B T} \right) S[\rho(\mathbf{r})]. \quad (8)$$

We used κ values corresponding to a Debye length of 3 Å, corresponding to a 1 M concentration of a 1:1 electrolyte ($c_0 = 1$ M). This mimics the experimental situation where 1 M of a strong acid is used ($U_{\text{SHE}} = 0$ for HER and pH = 0).

Though grand-canonical SCF algorithms exist²¹ which vary the number of electrons N_e so as to match the targeted chemical potential,

currently only conventional (canonical) methods are available in VASPsol, making it necessary to adjust N_e in between successive SCF loops instead. For local minimization runs, we use a simple iterative approach:

$$N_e(i+1) = N_e(i) - a \cdot [\mu_e(i) - \mu_{e,\text{target}}]. \quad (9)$$

We find an a value of 1.0 V⁻¹ to be appropriate for the structures considered in this work. In this manner, the electrode potential converges to the targeted value as the local optimization proceeds. For saddle point searches, we find it more convenient to adapt N_e after a completed dimer search, iterating until the target potential is matched within 15 mV.

The electronic chemical potential μ_e is calculated by comparing the Fermi level with the potential in the bulk electrolyte, which in an implicit solvent equals that of an electron in vacuum:²³

$$\mu_e = \epsilon_{\text{Fermi}} - V_{\text{bulk}}. \quad (10)$$

If, then, a certain potential U is to be attained w.r.t. the standard hydrogen electrode (SHE), the target chemical potential is given by:

$$\mu_{e,\text{target}} = -\Phi_{\text{SHE}} - U, \quad (11)$$

where Φ_{SHE} is the work function of the SHE. We have taken Φ_{SHE} equal to 4.43 V, which lies within the experimental value of the SHE work function compared to vacuum which is usually measured to be 4.44 (+/- 0.02) V.⁵³

To compare energy differences of two structures at different N_e values (but identical electrode potential U), the VASPsol and JDFTx output energies need to be corrected by the cost (gain) of removing (adding) electrons:

$$\Omega = E_{\text{DFT}} + N_e \mu_e(U). \quad (12)$$

Even though E_{DFT} here includes entropy terms from the solvation model, we will refer to $\Delta\Omega$ as (electronic) grand-canonical energy differences, as no entropic contributions are included from the explicit atom calculations.

The symmetry factor β for an elementary reaction at a given U corresponds to the deriva-

284 tive of the activation energy w.r.t. U , which
 285 we evaluate using a central difference scheme
 286 ($\Delta U = 0.1\text{V}$):

$$\beta(U) = \frac{\partial \Delta \Omega_{\text{act}}}{e \partial U}, \quad (13)$$

$$\approx \frac{\Delta \Omega_{\text{act}}(U + \Delta U) + \Delta \Omega_{\text{act}}(U - \Delta U)}{2e\Delta U}. \quad (14)$$

287 Results and Discussion

288 In the following paragraphs we present our re-
 289 sults for Volmer, Tafel, and Heyrovský energy
 290 barriers on Pt(111) and Pt(110) at $U = 0\text{ V}$ on
 291 the SHE scale.

292 H₂ evolution on Pt(111)

293 Convergence w.r.t. slab separation

294 The activation energies calculated with VASP-
 295 sol (following the procedure outlined in the pre-
 296 vious Section) are found to converge only slowly
 297 with respect to the distance L_z between period-
 298 ically repeated slabs. More precisely, the acti-
 299 vation energies are a linear function of $1/L_z$,
 300 as shown in Figure 2. The slopes of the fitted
 301 regression lines appear to be anti-correlated
 302 to the difference in N_e between the initial and
 303 transition states. The slope is namely close to
 304 zero for the Tafel reactions (for which $\Delta N_e \simeq$
 305 -0.05 e^-) and negative for the Volmer and Hey-
 306 rovský reactions (where $\Delta N_e \simeq 0.6\text{ e}^-$).

307 The $1/L_z$ dependence suggests the presence of
 308 spurious charge interactions in the conventional
 309 3D-periodic implementation in VASPsol. This
 310 behavior is possibly connected to the observa-
 311 tion that standard Poisson-Boltzmann models
 312 do not necessarily enforce strict charge neutral-
 313 ity.⁵⁴ We therefore performed single-point cal-
 314 culations using the JDFTx code which imple-
 315 ments a truncated Coulomb scheme to fully de-
 316 couple periodically repeated slabs.⁵⁵ As shown
 317 in Table 1, the JDFTx activation energies in-
 318 deed agree well with the VASPsol results ex-
 319 trapolated to $L_z = \infty$. The small differences
 320 that remain can be attributed to the different

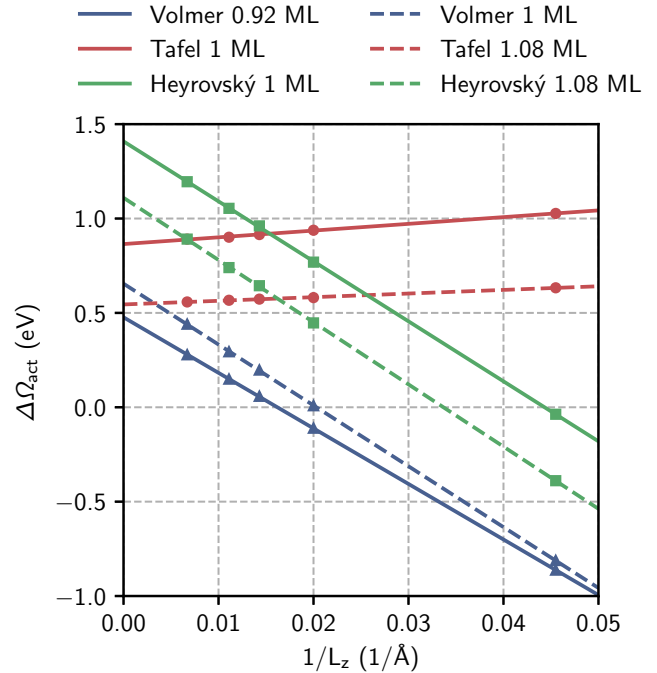


Figure 2: Activation energies calculated using VASPsol for HER reactions on Pt(111) using Eigen ions as a proton model for the PCET reactions. The values are plotted as function of the inverse of the cell length perpendicular to the plane of the slab. The three types of barriers have been evaluated at two different hydrogen coverages in the reactant state, i.e. at/below 1 ML and above 1 ML.

321 treatments of core-valence interactions and ki-
 322 netic energy cutoffs.

323 It should furthermore be noted that the
 324 L_z -dependence seems not to have been taken
 325 into account in several previous studies^{24,25,27}
 326 of PCET reactions using the VASPsol code.
 327 Without extrapolation to $L_z = \infty$, values of
 328 L_z of over 400 Å would be required
 329 in the present work to converge the Volmer and
 330 Heyrovský barriers on Pt(111) within 0.1 eV.

331 Water model

332 Figure 3 furthermore shows the barrier heights
 333 when an ice bilayer is used for the water struc-
 334 ture (red bars), compared to the results with an
 335 Eigen ion (blue bars).² The two sets are in fair

²Note that the Tafel barriers reported in the ‘water cluster’ approach are calculated without explicit water

Table 1: Comparison of VASPsol activation energies (extrapolated to $L_z = \infty$) and JDFTx single-point calculations performed at the VASPsol geometries using a Coulomb truncation scheme. Each barrier has been evaluated at two different initial hydrogen coverages θ_H as well as two different water structures (a water cluster corresponding to the ‘Eigen’ cation as well as the (protonated) ice bilayer (‘IBL’ structure)).

Reaction	θ_H (ML)	$\Delta\Omega_{\text{act}}$ (eV)			
		VASPsol (Eigen)	JDFTx (Eigen)	VASPsol (IBL)	JDFTx (IBL)
Volmer	0.92	0.477	0.479	0.692	0.693
	1.00	0.655	0.629	0.805	0.838
Tafel	1.00	0.865	1.007	0.807	0.830
	1.08	0.545	0.407	0.420	0.416
Heyrovský	1.00	1.408	1.364	1.618	1.625
	1.08	1.110	0.995	1.393	1.388

agreement, though it can be noticed that the barriers for the PCET reactions (i.e. Volmer and Heyrovský steps) are consistently increased by about 0.2 eV when employing the ice bilayer model. We attribute this difference to the relative rigidity of the bilayer structure, leading to a more pronounced loss (compared to the more ‘flexible’ water cluster model) of hydrogen bonds in the transition state than in the initial state. The changes in H-bond distances are reported in Table 2 for the Volmer reaction (the corresponding transition state structures are shown in Figure 1). For the water cluster, the coordination of the central H_3O^+ ion is qualitatively similar in the initial and transition states: 2 H-bonds are donated, and 1 H-bond is accepted. Using the ice bilayer, however, the H_3O^+ ion in the initial state is significantly less well solvated compared to the initial state: two fewer H-bonds are donated, and only one more (stretched) H-bond is accepted. Though the structural properties of the water/Pt(111) interface remains an active field of research, several theoretical and experimental works have provided support for ice bilayer formation on Pt(111).^{56–59} This suggests that the energy barrier obtained with the bilayer structure would be more accurate than with the cluster model. As will be discussed further below, however, the Volmer and Heyrovský steps are not kinetically

relevant for HER on Pt(111) at 0 V_{SHE} , and therefore the relative accuracy of the two water models cannot be compared in this context.

Table 2: Hydrogen-bond distances in Å for the H_3O^+ ion at the initial state (IS) and transition state (TS) for the Volmer step on Pt(111) with an initial H coverage of 0.92 ML.

Water structure	Donor	Acceptor
Water cluster (IS)	1.39, 1.39	2.09
Water cluster (TS)	1.75, 1.80	1.94
Ice bilayer (IS)	1.45, 1.59, 1.58	-
Ice bilayer (TS)	1.70	2.46

Comparison with the extrapolation approach

The calculated barrier heights are now compared with literature results obtained with the extrapolation at the same electrode potential, hydrogen coverage, and water model (the ice bilayer structure, see Ref. 6) as also shown in Figure 3.³ The agreement is remarkably good, considering the pronounced differences in method-

³In Ref. 6 the Heyrovský barrier at an initial H coverage of 1 ML is given at -0.2 V_{SHE} . We therefore used a typical symmetry factor of 0.5 to estimate the corresponding value at 0 V_{SHE} .

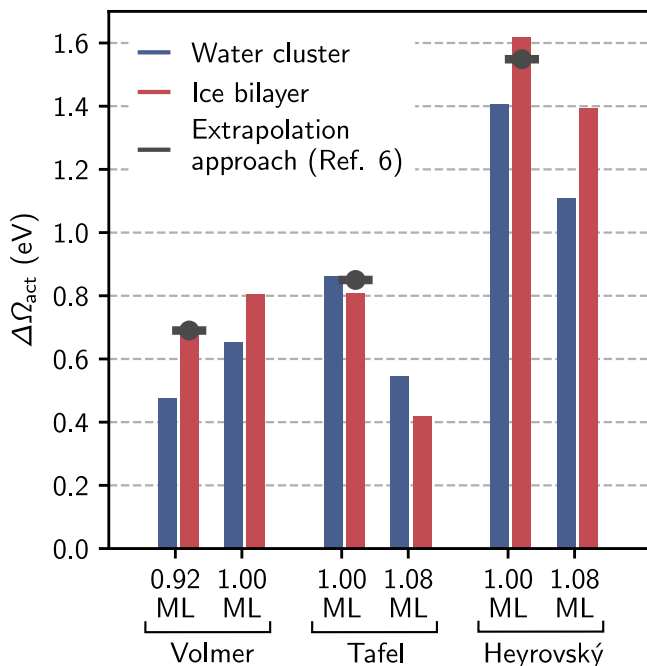


Figure 3: Calculated activation energies for HER reactions on Pt(111) using the implicit solvation scheme (VASPsol) at different initial hydrogen coverages and with two different water structures. The values obtained via the extrapolation approach are also indicated (see Ref. 6)

ology. Both approaches therefore agree that hydrogen is evolved via a Volmer-Tafel mechanism with the Tafel step as the RDS.

Additionally, Figure 3 shows that with the implicit solvation approach the barriers change as the coverage is increased beyond 1 ML, in ways which are similar to the extrapolation approach.⁶ Increasing the coverage beyond 1 ML requires the occupation of the energetically less favorable atop sites. Following a Bell-Evans-Polanyi principle, the activation energy for the Volmer step increases, whereas those of the Tafel and Heyrovský steps decrease.

Lastly, the symmetry factors β calculated at 0 V_{SHE} with the ice bilayer model amount to 0.62 (Volmer, $\theta_H = 0.92$ ML), -0.04 (Tafel, $\theta_H = 1$ ML), and 0.76 (Heyrovský, $\theta_H = 1$ ML). The activation energies of the two PCET reactions will therefore indeed decrease as the applied potential is lowered, while the barrier for the non-electrochemical Tafel step is nearly potential-independent. Skúlason and cowork-

ers⁶ obtained values of 0.44, ~ 0 , and 1.07, respectively, using the extrapolation approach. These values are, however, not directly comparable to ours, as these also include the potential dependence of the hydrogen coverage and of the transition state geometry and are obtained by linear regression over a fairly wide potential range of 1 V or more.

Comparison with experimental measurements

Experimental measurements of the HER kinetics on Pt(111) surfaces are available in the works by Marković et al.³⁵ and He et al.⁶⁰ Although both groups measure similar current densities at 0 V, different temperature dependencies are reported. We follow the explanation offered in Ref. 60 that the Pt(111) substrate used in Ref. 35 may have contained low concentrations of highly active defect sites. In this view, the higher apparent activation energy measured by He et al. (circa 0.67 eV) should be closer to that of a pristine Pt(111) surface. The magnitude of the corresponding pre-exponential factor (circa 10^{10} mA/cm²) is characteristic of a process involving only surface adsorbates, supporting the Tafel reaction as the RDS. These findings compare well with the computational results described in the previous paragraphs. As the barrier for the Tafel step is not sensitive to the water structure at the interface, this does not, unfortunately, allow to discriminate between different types of water models.

Comparison with other implicit solvent calculations

Fang et al. have previously addressed³¹ the HER on Pt(111) using a largely similar method implemented in the SIESTA code.^{32,33} At 0 V_{SHE} and a hydrogen coverage at or below 1 ML, the Tafel barrier reported by Fang et al. (0.92 eV) agrees well with our calculations, while the reported Volmer and Heyrovský barrier heights are significantly lower than ours (< 0.2 eV and 0.93 eV, respectively). We presume the origins of this difference may lie in

the DFT setup, details of the implicit solvation model, the use of a water trimer cluster (as opposed to the quadrimer employed here), and/or the inclusion of entropic and zero-point vibrational contributions (which are not considered here).

An alternative constant-potential implicit solvation approach has been recently proposed³⁴ where essentially the countercharge is not described by a Poisson-Boltzmann equation, but is instead homogeneously spread out over the bulk solvent region. Using this ‘solvated jellium method’ (SJM), the barrier for the Volmer step on Pt(111) is found to be significantly lower (circa 0.02 eV at 0 V_{SHE} using the ice bilayer model, compared to 0.7 eV in the present work). Also here further investigation is needed to locate the origin of the discrepancy, i.e. whether or not it is due to the simplified description of the countercharge distribution. One important question is whether the SJM energy differences change as the jellium+solvent width is increased, which entails a progressive dilution of the countercharge concentration.

H₂ evolution on Pt(110)-(1×2)

We now turn to the missing-row reconstructed Pt(110) surface, with a hydrogen coverage of 1 ML where all ridge and (micro-)facet sites are occupied (see Panel (b) in Figure 4). Although there is a weak thermodynamic preference for the adsorption of additional hydrogen atoms in the trough sites at $U_{\text{SHE}} = 0$ V (with differential binding energies of circa 0.1 eV),^{6,61,62} it will be argued below that trough-adsorbed hydrogen atoms, if present, would not contribute significantly to the hydrogen evolution rate at 0 V.

Panel (a) in Figure 4 shows the calculated barrier heights for several relevant Volmer and Tafel steps at and below 1 ML coverage of hydrogen. Various attempts at locating saddle points for the Heyrovský reactions converged to Volmer-like saddle points, suggesting that these reactions are inoperable on this surface. On both sites the Tafel reaction proceeds via an intermediate corresponding to a Kubas complex,⁶³ consisting of a stretched hydrogen

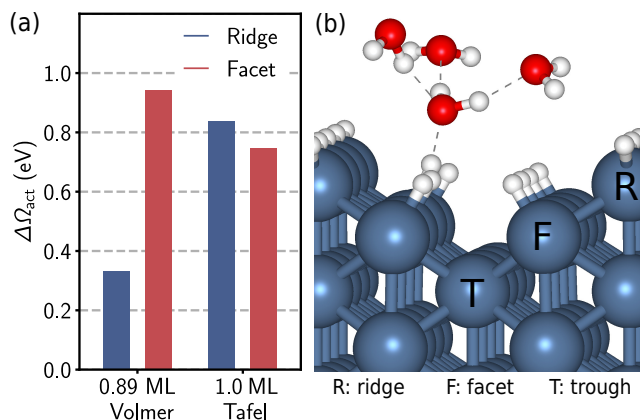


Figure 4: Panel (a): calculated barrier heights for the Volmer and Tafel processes on the Pt(110)-(1×2) surface. Panel (b): structural model of the transition state for the Volmer reaction on a (micro-)facet.

molecule on top of a platinum atom (see Figure 5). Desorption of H₂ via the Tafel reaction is faster on the facet (0.75 eV) compared to the ridge (0.84 eV). This is in line with the higher binding energy of the ridge-bound adatoms. These results are comparable to calculations in the literature using the same functional and hydrogen coverage, but without solvent and at the potential of zero charge.^{6,62}

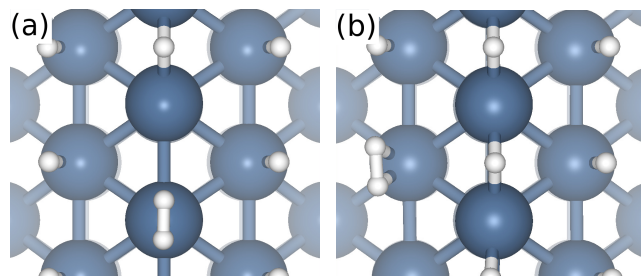


Figure 5: Structural models of the Kubas complex as an intermediate of the Tafel reaction on ridges (a) and microfacets (b) of the Pt(110)-(1×2) surface.

Similarly, at an initial hydrogen coverage of 0.89 ML, we find a higher barrier for the Volmer step on the facets (0.94 eV) compared to the ridge (0.33 eV). This change exceeds the difference in hydrogen binding energy between the two site types (calculated to be only 0.23 eV). Hence, even though hydrogen desorption will take place on the facets, replenishment of the coverage happens most rapidly via diffusion of

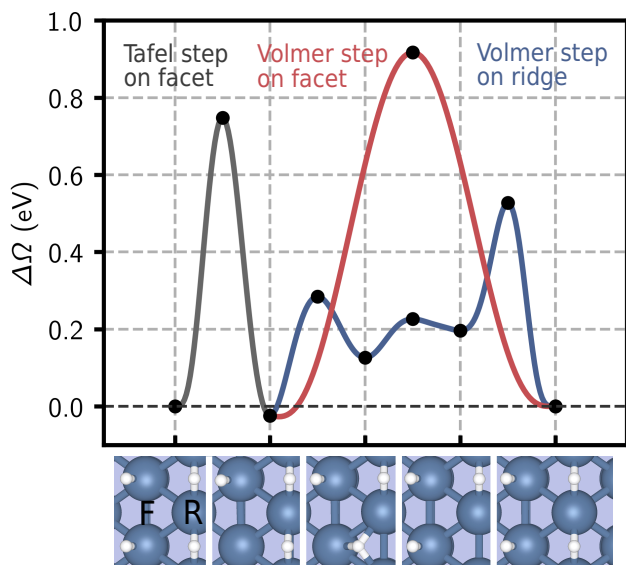


Figure 6: Calculated energy diagram for HER on Pt(110)-(1 \times 2) for a steady-state hydrogen coverage of 1 ML. The reaction energies have been evaluated using the CHE formalism.

H atoms from the ridge to the vacant facet sites followed by Volmer discharge on the now-vacant ridge site. This process is illustrated in the energy diagram in Figure 6. As the diffusion barrier is low (0.3 eV), the Volmer step will dictate the apparent activation energy, which then amounts to 0.56 eV. This entails that hydrogen deposition is fast relative to the Tafel reaction, making the latter the rate-determining step. This mechanism, as well as the lower barrier of the rate-limiting Tafel step compared to Pt(111), is in good agreement with the measurements on Pt single crystal surfaces by Marković and coworkers.³⁵

We now return to the question whether hydrogen coverages beyond 1 ML (with occupations of trough sites) could be relevant at $U = 0$ V_{SHE}. Firstly, the relatively high barrier obtained for the Volmer reaction on the facet suggests that the corresponding barrier on the trough will be even higher, requiring a similar diffusion-assisted mechanism as described above. However, moving a ridge-bound H atom to a trough position requires more energy (0.46 eV) than to a facet site. Achieving a significant occupation of the trough sites is, therefore, kinetically difficult. Additionally, even if a partial occupation of the trough sites would be

reached, the Tafel reaction on the facets would remain the main desorption pathway for hydrogen. Previous studies have namely found that, despite the lower binding energy, the barrier for hydrogen desorption from trough sites is larger compared to the facet sites when the hydrogen coverage is at or slightly beyond 1 ML.^{61,62} It is therefore sufficient to only consider ridge- and facet-bound hydrogen atoms for HER on Pt(110)-(1 \times 2) at 0 V_{SHE}.

Conclusions

We have evaluated the performance of a recently developed constant-potential implicit solvation approach to electrochemical barriers for one of the classical processes in catalysis, the hydrogen evolution reaction on platinum. The relevant Volmer, Tafel, and Heyrovský kinetics on Pt(111) and Pt(110) at 0 V versus SHE compare well with the previously developed ‘extrapolation’ approach and with available experimental data. Importantly, the inclusion of an implicit solvent only moderately increases the computational cost, whereas calculating barrier heights with the extrapolation approach is more expensive by at least one order of magnitude. Care should be taken, however, in dealing with spurious electrostatic interactions between periodically repeated slabs when using the VASPsol code.

Although further testing for other types of reactions and materials is warranted, we have so far found the accuracy to be satisfactory and expect implicit solvation approaches to receive increasing attention in future research. The application and continued development of cost-effective methods is most welcome, as the previous lack of such approaches has frequently led to kinetic aspects being disregarded in first-principles electrocatalysis research.

Acknowledgement The authors thank Vitae Industries for providing computational resources, and Javed Hussain for valuable discussions. This material is based upon work supported by the National Science Foundation under Grant No. CHE-1665372.

Supporting Information Available

Coordinate files pertaining to the hydrogen evolution reactions on Pt(111) and Pt(110).

References

- (1) Nørskov, J. K.; Rossmeisl, J.; Logadottir, A.; Lindqvist, L.; Kitchin, J. R.; Bligaard, T.; Jónsson, H. Origin of the Overpotential for Oxygen Reduction at a Fuel-Cell Cathode. *J. Phys. Chem. B* **2004**, *108*, 17886–17892.
- (2) Nørskov, J. K.; Bligaard, T.; Logadottir, A.; Kitchin, J. R.; Chen, J. G.; Pandelov, S.; Stimming, U. Trends in the Exchange Current for Hydrogen Evolution. *J. Electrochem. Soc.* **2005**, *152*, J23–J26.
- (3) Skúlason, E.; Jónsson, H. Atomic scale simulations of heterogeneous electrocatalysis: recent advances. *Adv. Phys. X* **2017**, *2*, 481–495.
- (4) Exner, K. S.; Over, H. Kinetics of Electrocatalytic Reactions from First-Principles: A Critical Comparison with the Ab Initio Thermodynamics Approach. *Acc. Chem. Res.* **2017**, *50*, 1240–1247.
- (5) Rossmeisl, J.; Skúlason, E.; Björketun, M. E.; Tripkovic, V.; Nørskov, J. K. Modeling the electrified solid-liquid interface. *J. Chem. Phys. Lett.* **2008**, *466*, 68–71.
- (6) Skúlason, E.; Tripkovic, V.; Björketun, M. E.; Gudmundsdóttir, S.; Karlberg, G.; Rossmeisl, J.; Bligaard, T.; Jónsson, H.; Nørskov, J. K. Modeling the Electrochemical Hydrogen Oxidation and Evolution Reactions on the Basis of Density Functional Theory Calculations. *J. Phys. Chem. C* **2010**, *114*, 18182–18197.
- (7) Skúlason, E.; S. Karlberg, G.; Rossmeisl, J.; Bligaard, T.; Greeley, J.; Jónsson, H.; K. Nørskov, J. Density functional theory calculations for the hydrogen evolution reaction in an electrochemical double layer on the Pt(111) electrode. *Phys. Chem. Chem. Phys.* **2007**, *9*, 3241–3250.
- (8) Hussain, J.; Jónsson, H.; Skúlason, E. Faraday efficiency and mechanism of electrochemical surface reactions: CO₂ reduction and H₂ formation on Pt(111). *Faraday Discuss.* **2016**, *195*, 619–636.
- (9) Hussain, J.; Jónsson, H.; Skúlason, E. Calculations of Product Selectivity in Electrochemical CO₂ Reduction. *ACS Catal.* **2018**, 5240–5249.
- (10) Chan, K.; Nørskov, J. K. Electrochemical Barriers Made Simple. *J. Phys. Chem. Lett.* **2015**, *6*, 2663–2668.
- (11) Chan, K.; Nørskov, J. K. Potential Dependence of Electrochemical Barriers from ab Initio Calculations. *J. Phys. Chem. Lett.* **2016**, *7*, 1686–1690.
- (12) Filhol, J.-S.; Neurock, M. Elucidation of the Electrochemical Activation of Water over Pd by First Principles. *Angew. Chem. Int. Ed.* **2006**, *45*, 402–406.
- (13) Taylor, C. D.; Wasileski, S. A.; Filhol, J.-S.; Neurock, M. First principles reaction modeling of the electrochemical interface: Consideration and calculation of a tunable surface potential from atomic and electronic structure. *Phys. Rev. B* **2006**, *73*, 165402.
- (14) Makov, G.; Payne, M. C. Periodic boundary conditions in ab initio calculations. *Phys. Rev. B* **1995**, *51*, 4014–4022.
- (15) Komsa, H.-P.; Rantala, T. T.; Pasquarello, A. Finite-size supercell correction schemes for charged defect calculations. *Phys. Rev. B* **2012**, *86*, 045112.
- (16) Otani, M.; Hamada, I.; Sugino, O.; Morikawa, Y.; Okamoto, Y.; Ikeshoji, T.

Structure of the water/platinum interface – a first principles simulation under bias potential. *Phys. Chem. Chem. Phys.* **2008**, *10*, 3609–3612.

(17) Surendralal, S.; Todorova, M.; Finnis, M. W.; Neugebauer, J. First-Principles Approach to Model Electrochemical Reactions: Understanding the Fundamental Mechanisms behind Mg Corrosion. *Phys. Rev. Lett.* **2018**, *120*, 246801.

(18) Akhade, S. A.; Bernstein, N. J.; Esopi, M. R.; Regula, M. J.; Janik, M. J. A simple method to approximate electrode potential-dependent activation energies using density functional theory. *Catal. Today* **2017**, *288*, 63–73.

(19) Akhade, S. A.; Nidzyn, R. M.; Rostamikia, G.; Janik, M. J. Using Brønsted-Evans-Polanyi relations to predict electrode potential-dependent activation energies. *Catal. Today* **2018**, *312*, 82–91.

(20) Sundararaman, R.; Goddard, W. A.; Arias, T. A. Grand canonical electronic density-functional theory: Algorithms and applications to electrochemistry. *J. Chem. Phys.* **2017**, *146*, 114104.

(21) Sundararaman, R.; Letchworth-Weaver, K.; Schwarz, K. A.; Gunceler, D.; Ozhabes, Y.; Arias, T. A. JDFTx: Software for joint density-functional theory. *SoftwareX* **2017**, *6*, 278–284.

(22) Mathew, K.; Sundararaman, R.; Letchworth-Weaver, K.; Arias, T. A.; Hennig, R. G. Implicit solvation model for density-functional study of nanocrystal surfaces and reaction pathways. *J. Chem. Phys.* **2014**, *140*, 084106.

(23) Mathew, K.; Hennig, R. G. Implicit self-consistent description of electrolyte in plane-wave density-functional theory. *arXiv:1601.03346 [cond-mat]* **2016**, arXiv: 1601.03346.

(24) Goodpaster, J. D.; Bell, A. T.; Head-Gordon, M. Identification of Possible Pathways for C-C Bond Formation during Electrochemical Reduction of CO₂: New Theoretical Insights from an Improved Electrochemical Model. *J. Phys. Chem. Lett.* **2016**, *7*, 1471–1477.

(25) Singh, M. R.; Goodpaster, J. D.; Weber, A. Z.; Head-Gordon, M.; Bell, A. T. Mechanistic insights into electrochemical reduction of CO₂ over Ag using density functional theory and transport models. *PNAS* **2017**, *114*, E8812–E8821.

(26) Garza, A. J.; Bell, A. T.; Head-Gordon, M. Is Subsurface Oxygen Necessary for the Electrochemical Reduction of CO₂ on Copper? *J. Phys. Chem. Lett.* **2018**, *9*, 601–606.

(27) Garza, A. J.; Bell, A. T.; Head-Gordon, M. Mechanism of CO₂ Reduction at Copper Surfaces: Pathways to C₂ Products. *ACS Catal.* **2018**, *8*, 1490–1499.

(28) Schwarz, K. A.; Sundararaman, R.; Mofat, T. P.; Allison, T. C. Formic acid oxidation on platinum: a simple mechanistic study. *Phys. Chem. Chem. Phys.* **2015**, *17*, 20805–20813.

(29) Wang, H.-F.; Liu, Z.-P. Formic Acid Oxidation at Pt/H₂O Interface from Periodic DFT Calculations Integrated with a Continuum Solvation Model. *J. Phys. Chem. C* **2009**, *113*, 17502–17508.

(30) Fang, Y.; Liu, Z. Electrochemical reactions at the electrode/solution interface: Theory and applications to water electrolysis and oxygen reduction. *Sci. China Chem.* **2010**, *53*, 543–552.

(31) Fang, Y.-H.; Wei, G.-F.; Liu, Z.-P. Catalytic Role of Minority Species and Minority Sites for Electrochemical Hydrogen Evolution on Metals: Surface Charging, Coverage, and Tafel Kinetics. *J. Phys. Chem. C* **2013**, *117*, 7669–7680.

- (32) Fang, Y.-H.; Wei, G.-F.; Liu, Z.-P. Theoretical modeling of electrode/electrolyte interface from first-principles periodic continuum solvation method. *Catal. Today* **2013**, *202*, 98–104.
- (33) Fang, Y.-H.; Liu, Z.-P. Tafel Kinetics of Electrocatalytic Reactions: From Experiment to First-Principles. *ACS Catal.* **2014**, *4*, 4364–4376.
- (34) Kastlunger, G.; Lindgren, P.; Peterson, A. A. Controlled-Potential Simulation of Elementary Electrochemical Reactions: Proton Discharge on Metal Surfaces. *J. Phys. Chem. C* **2018**,
- (35) Marković, N. M.; Grgur, B. N.; Ross, P. N. Temperature-Dependent Hydrogen Electrochemistry on Platinum Low-Index Single-Crystal Surfaces in Acid Solutions. *J. Phys. Chem. B* **1997**, *101*, 5405–5413.
- (36) Kresse, G.; Hafner, J. Ab Initio Molecular-Dynamics Simulation of the Liquid-Metal-Amorphous-Semiconductor Transition in Germanium. *Phys. Rev. B* **1994**, *49*, 14251–14269.
- (37) Kresse, G.; Furthmüller, J. Efficiency of Ab-Initio Total Energy Calculations for Metals and Semiconductors Using a Plane-Wave Basis Set. *Comp. Mater. Sci.* **1996**, *6*, 15–50.
- (38) Kresse, G.; Furthmüller, J. Efficient Iterative Schemes for Ab Initio Total-Energy Calculations Using a Plane-Wave Basis Set. *Phys. Rev. B* **1996**, *54*, 11169–11186.
- (39) Kresse, G.; Joubert, D. From ultra-soft pseudopotentials to the projector augmented-wave method. *Phys. Rev. B* **1999**, *59*, 1758–1775.
- (40) Hohenberg, P.; Kohn, W. Inhomogeneous Electron Gas. *Phys. Rev.* **1964**, *136*, B864–B871.
- (41) Kohn, W.; Sham, L. J. Self-Consistent Equations Including Exchange and Correlation Effects. *Phys. Rev.* **1965**, *140*, A1133–A1138.
- (42) Garrity, K. F.; Bennett, J. W.; Rabe, K. M.; Vanderbilt, D. Pseudopotentials for high-throughput DFT calculations. *Comp. Mater. Sci.* **2014**, *81*, 446–452.
- (43) Hammer, B.; Hansen, L. B.; Nørskov, J. K. Improved adsorption energetics within density-functional theory using revised Perdew-Burke-Ernzerhof functionals. *Phys. Rev. B* **1999**, *59*, 7413–7421.
- (44) Perdew, J. P.; Burke, K.; Ernzerhof, M. Generalized Gradient Approximation Made Simple. *Phys. Rev. Lett.* **1996**, *77*, 3865–3868.
- (45) Marques, M. A. L.; Oliveira, M. J. T.; Burnus, T. Libxc: A library of exchange and correlation functionals for density functional theory. *Computer Physics Communications* **2012**, *183*, 2272–2281.
- (46) Monkhorst, H. J.; Pack, J. D. Special points for Brillouin-zone integrations. *Phys. Rev. B* **1976**, *13*, 5188–5192.
- (47) Pack, J. D.; Monkhorst, H. J. ‘Special points for Brillouin-zone integrations’ – a reply. *Phys. Rev. B* **1977**, *16*, 1748–1749.
- (48) Henkelman, G.; Jónsson, H. Improved tangent estimate in the nudged elastic band method for finding minimum energy paths and saddle points. *J. Chem. Phys.* **2000**, *113*, 9978–9985.
- (49) Henkelman, G.; Jónsson, H. A dimer method for finding saddle points on high dimensional potential surfaces using only first derivatives. *J. Chem. Phys.* **1999**, *111*, 7010–7022.
- (50) Gunceler, D.; Letchworth-Weaver, K.; Sundararaman, R.; Schwarz, K. A.; Arias, T. A. The importance of nonlinear fluid response in joint density-functional theory studies of battery systems. *Modelling Simul. Mater. Sci. Eng.* **2013**, *21*, 074005.

- (51) Andreussi, O.; Dabo, I.; Marzari, N. Revised self-consistent continuum solvation in electronic-structure calculations. *J. Chem. Phys.* **2012**, *136*, 064102.
- (52) Murrell, J.; Jenkins, A. *Properties of liquids and solutions*, 2nd ed.; Wiley & Sons: Chichester, England, 1994.
- (53) Trasatti, S. The absolute electrode potential: an explanatory note (Recommendations 1986). *Pure Appl. Chem.* **1986**, *58*, 955–966.
- (54) Melander, M.; Kuisma, M.; Christensen, T.; Honkala, K. *Grand-Canonical Approach to Density Functional Theory of Electrocatalytic Systems: Thermodynamics of Solid-Liquid Interfaces at Constant Ion and Electrode Potentials*; ChemRxiv, 2018.
- (55) Sundararaman, R.; Arias, T. A. Regularization of the Coulomb singularity in exact exchange by Wigner-Seitz truncated interactions: Towards chemical accuracy in nontrivial systems. *Phys. Rev. B* **2013**, *87*, 165122.
- (56) Meng, S.; Xu, L. F.; Wang, E. G.; Gao, S. Vibrational Recognition of Hydrogen-Bonded Water Networks on a Metal Surface. *Phys. Rev. Lett.* **2002**, *89*, 176104.
- (57) Ogasawara, H.; Brena, B.; Nordlund, D.; Nyberg, M.; Pelmenschikov, A.; Pettersson, L. G. M.; Nilsson, A. Structure and Bonding of Water on Pt(111). *Phys. Rev. Lett.* **2002**, *89*, 276102.
- (58) Schnur, S.; Groß, A. Properties of metal-water interfaces studied from first principles. *New J. Phys.* **2009**, *11*, 125003.
- (59) Groß, A.; Gossenberger, F.; Lin, X.; Naderian, M.; Sakong, S.; Roman, T. Water Structures at Metal Electrodes Studied by Ab Initio Molecular Dynamics Simulations. *J. Electrochem. Soc.* **2014**, *161*, E3015–E3020.
- (60) He, Z.-D.; Wei, J.; Chen, Y.-X.; Santos, E.; Schmickler, W. Hydrogen evolution at Pt(111) - activation energy, frequency factor and hydrogen repulsion. *Electrochim. Acta* **2017**, *255*, 391–395.
- (61) Gudmundsdóttir, S.; Skúlason, E.; Jónsson, H. Reentrant Mechanism for Associative Desorption: H₂/Pt(110)-(1×2). *Phys. Rev. Lett.* **2012**, *108*, 156101.
- (62) Gudmundsdóttir, S.; Skúlason, E.; Weststrate, K.-J.; Juurlink, L.; Jónsson, H. Hydrogen adsorption and desorption at the Pt(110)-(1×2) surface: experimental and theoretical study. *Phys. Chem. Chem. Phys.* **2013**, *15*, 6323–6332.
- (63) Kubas, G. J. Molecular hydrogen complexes: coordination of a σ bond to transition metals. *Acc. Chem. Res.* **1988**, *21*, 120–128.

895

